THE ASTROPHYSICAL JOURNAL, 303:198–215, 1986 April 1

GAS IN AND TOWARD THE MAGELLANIC CLOUDS

A. SONGAILA,[1] J. C. BLADES,[2] AND E. M. HU[1]
Space Telescope Science Institute
AND
L. L. COWIE[1,3]
Space Telescope Science Institute; and Physics and Astronomy Department, Johns Hopkins University
Received 1985 July 1; accepted 1985 September 30

ABSTRACT

We present Ca II K absorption spectra, at resolutions of 8–17 km s^{-1}, of 48 early-type supergiants in the Large and Small Magellanic Clouds. These observations were obtained to address two specific issues: the possible fragmentary nature of the Clouds (particularly the SMC), and the distance to the gas responsible for the absorption lines at 60 and 120 km s^{-1} (LSR) seen in UV spectra of Magellanic Cloud stars by Savage and de Boer. By comparing our spectra with H I measurements toward the Clouds, we come to the following conclusions. First, it is clear that, in both Clouds, velocity components in the neutral hydrogen distribution lie at different distances along the line of sight. We also find that there is lower column density material, similar to the 60 and 120 km s^{-1} features, which can be demonstrated to lie within the Clouds. Given the presence of weakly absorbing gas within the Clouds themselves, there seems no compelling reason to assign the very similar 60 and 120 km s^{-1} weak absorption features to the halo of our own Galaxy, as Savage and de Boer assumed; the simplest assumption is that all the weak absorption along the line of sight arises in low column density material within the Magellanic Clouds.

We find good agreement between the spread in radial velocity shown in absorbing material and the radial velocity spread predicted by Murai and Fujimoto's dynamical model of the formation of the Magellanic Stream by tidal stripping. An elongated and somewhat disrupted SMC arises naturally in these simulations as a result of the tidal interaction of the LMC and SMC that is presumed to have given rise to the Magellanic Stream. These models predict a large spread in distance to the Clouds (and particularly the SMC), and we point out that this result is in fact highly model-independent. We therefore speculate, following Mathewson and Ford's discussion of the SMC, that both the LMC and the SMC are extended and fragmented along the line of sight.

Subject headings; galaxies: Magellanic Clouds — interstellar: matter — radial velocities

I. INTRODUCTION

Over the past five years, we have collected a substantial number of high-resolution optical absorption-line spectra of stars in the Magellanic Clouds. Spectra of 30 early-type supergiants in the LMC and 18 in the SMC have been obtained at resolutions of 8–17 km s^{-1} at Ca II H and K (and in some cases at Na I D). This large and uniform set of data complements the H I surveys of the Clouds, (McGee and Milton 1966*b*; Hindman 1967; Mathewson *et al.* 1979; Rohlfs *et al.* 1984) and the lower resolution ($\sim$60 km s^{-1}) optical absorption-line work published by Feast, Thackeray, and Wesselink (1960) and more recently by Cohen (1984). The present paper is intended to provide an overall view of this new data and to answer a number of specific questions. A full spectral atlas will be published separately.

The data are well suited to answer two questions which to our mind are of crucial importance in understanding the Magellanic Cloud gas. These questions are: (1) are the Clouds fragmented along the line of sight, as Mathewson and Ford (1984) have suggested for the SMC; and (2) what is the location along the line of sight of the weak absorption features found in the UV by Savage and de Boer (1979, 1981)?

In § II we describe the observations and in § III we present an overview of the optical absorption-line data and their relation to neutral hydrogen observations. These Ca II absorption line measurements are more sensitive to the presence of gas than the early neutral hydrogen surveys and show both strong absorption lines, attributable to the major gas features in the Clouds, which are also seen in 21 cm emission, and weaker absorption lines with a much wider velocity spread, which are not. The weak absorption features, a category which includes the Savage and de Boer intermediate-velocity material, can be seen in more sensitive 21 cm observations and have column densities of around a few times 10^{18} cm^{-2} in H I (McGee, Newton, and Morton 1983).

Combining neutral hydrogen and optical absorption-line data is a very powerful technique for studying the spatial distribution of gas toward the Clouds. By comparing the distribution of neutral hudrogen with that of the more sensitive calcium, we can decide which 21 cm features are foreground and which are background. This comparison shows that the velocity peaks seen in the neutral hydrogen are spatially layered: the gas appears to lie at various distances, with some velocity components showing in absorption in all stars, while others disappear in the spectra of what are presumably fore-

[1] Visiting Astronomer, Cerro Tololo Inter-American Observatory, which is operated by AURA, Inc., under contract with the National Science Foundation.
[2] Affiliated to the Astrophysics Division, Space Science Department of ESA.
[3] Alfred P. Sloan Foundation Fellow.

ground stars. Weak absorption features are spatially interspersed among the stronger features.

In § IV we summarize the physical constraints which can be obtained from the information in § III. The answers to our two questions are: (1) Both the LMC and SMC appear to consist of layers at different velocities and distances. Whether these should be considered separate fragments remains unclear, and detailed determinations for all the sample stars would be of great interest in finding the separation of the material. (2) Certainly some fraction of, and probably all of, the weak absorption features seen in the spectra of the Cloud stars arise within the Clouds themselves, though it remains possible that some of these components are formed by halo absorption in our own Galaxy.

Finally, we consider whether the peculiar spatial and kinematic structure of the Clouds that we have inferred is reasonable in light of current models of the Clouds and Magellanic Stream. We have concentrated on comparing our calcium absorption-line measurements with Murai and Fujimoto's (1980) simulation of the Magellanic Cloud interaction and Magellanic Stream formation. The kinematic agreement is good, but this simulation also implies a spread in distance modulus of 0.5–0.9 mag in the SMC. We emphasize that this is not strictly a model-dependent result: the observed spread in radial velocities within the Clouds will almost inevitably result in such a distance spread. Mathewson's two-galaxy model of the SMC is the simplest scenario in which this is explicitly taken into account. Such effects could greatly complicate interpretation of distance measurements in the Magellanic Clouds, and distance moduli measured for individual objects or classes of objects may deviate significantly (by as much as 0.5 mag) from the average in a given region. Combination of direct distance estimates with the velocity-distance information inherent in the present data might be of great interest, but the results suggest that this will be an extremely difficult experiment.

II. OBSERVATIONS

The set of spectra for 48 early-type supergiants in the Magellanic Clouds which we shall use in this paper is the result of a number of years' observing by all the authors. Some of this work has been reported in full already, and the details need not be repeated here. Spectra of 11 stars, chosen to be widely distributed across the faces of both clouds, have been described by Songaila and York (1980) and Songaila, Cowie, and York (1981) and analyzed in Songaila (1981*b*). Blades (1980) and Blades and Meaburn (1980) have analyzed spectra of three supergiants in the 30 Doradus nebula. The remainder of the data is previously unpublished and consists of spectra of LMC and SMC stars, taken by one of us (J. C. B.) with the image photon counting system (IPCS) at the Anglo-Australian Telescope (AAT), spectra of stars in the LMC and SMC taken by one of us (E. M. H.) at CTIO, and chosen to be behind or near the line of sight to known supernova remnants, and spectra of stars in the LMC taken at CTIO by two of us (A. S., and L. L. C) and chosen to provide small-scale angular coverage around a number of the previously observed stars.

All the spectra were taken with one or other of two basic instrument combinations: (1) the CTIO 4 m telescope with the echelle spectrograph recorded with either the Singer image tube camera or the long focal length blue camera plus image tube on baked IIIa-J or IIa-O plates; (2) the Anglo-Australian Telescope with the RGO spectrograph and 82 cm camera, recorded with the IPCS.

The CTIO echelle was operated in most cases with its 79 lines mm^{-1} echelle grating and cross-disperser 226-2 optimized to center wavelengths around calcium K λ3933.663.A $CuSO_4$ filter was used to block red light from the first order of the cross disperser. (In a few early spectra, a different configuration was used to allow the simultaneous recording of calcium K and sodium D λ5890; see Songaila and York 1980 for details,) Intensity calibration was made using the spot sensitometer on separate plates exposed to as uniform a density as possible for the same exposure time as the stellar spectrum. The spectrograph slit was normally set to $1'' \times 10''$. The resulting resolutions are 17 km s^{-1} with the Singer camera and ~ 8 km s^{-1} with the long-focus blue camera, as measured for emission lines of thorium-argon comparison lamp exposures taken before and after each stellar exposure. All stars were trailed along the slit during exposure.

The AAT spectra at Ca K were obtained with the 82 cm camera and the RGO spectrograph operating with grating 1200R in second order. This format gives a wavelength coverage of ~ 150 Å at a dispersion of 5 mm^{-1}. The final resolution was ~ 15 km s^{-1}, very similar to the CTIO lower resolution spectra. Wavelength calibration was made by means of a copper-argon comparison lamp exposed before and after each stellar spectrum. Spectra of 15 stars in the SMC and three in the LMC were also made at a wavelength near sodium D, using grating 1200R in first order to give a resolution of 10 mm^{-1}.

The photographic spectra were digitized with the PDS microdensitometer at Kitt Peak National Observatory and reduced to one-dimensional sky-subtracted spectra using the FSTSCN and ECHORD programs either at KPNO or at Princeton University. The regions of interest around the lines of calcium K and H were wavelength-calibrated by linearly interpolating from nearby comparison arc lines, and corrections were made for Earth's orbital velocity and for the motion of the Sun with respect to the local standard of rest. The spectra were then flattened over a region of $\sim \pm 500$ km s^{-1}, measured from the zero velocity of the lines of interest, by dividing by a polynomial continuum of order 3 or less fitted to this portion of the stellar continuum. The IPCS spectra were reduced using SDRSYS at the AAT. Wavelength calibration was carried out by making, typically, a fifth- or seventh-order fit to about 30 calibration lines fairly uniformly spread along the entire spectrum. The spectra were then velocity-corrected and flattened in the same way as the photographic spectra. Finally, spectra of the same star were averaged, after rebinning by linear interpolation to a common velocity scale, and smoothed using a three-point box filter.

Although obtained in such different ways, the spectra from the two sources are extremely similar, providing an excellent check on the accuracy of the two different instrument combinations used here, and also on the reduction procedures. As an example, Figure 3*b* shows a number of different spectra of the star R112 in the LMC, which will be described more fully in § III. The second spectrum from the top was obtained with the IPCS, while the remaining two were obtained with the CTIO echelle. The velocities of the principal absorption components agree to within 5 km s^{-1}, which is larger than the residuals of the wavelength fit, typically ~ 1 km s^{-1}, and is a better representation of the limiting velocity accuracy. Similarly, the equivalent widths of the main features agree to within

TABLE 1

MAGELLANIC CLOUD STELLAR DATA

R (1)	Sk (2)	Other (3)	R.A. (1950.0) (4)	Decl. (1950.0) (5)	V (6)	Sp. (7)	RV (km s^{-1}) (8)	Associated Nebulosity (9)
				Large Magellanic Cloud				
53	5–67	268605	04^{h}50^{m}20^s.4	−67°44′36″	11.34	B0Ia	260, 294	N3, DEM 7
55	16–69	268718	04 52 14.6	−69 30 24	10.72	B9Ia	..., 253	N79, DEM 10[a]
71	3–71	269006	05 02 46.1	−71 24 27	9.83	Pec	..., 180	= Henize S155
74	41–67	268939	05 04 15.4	−67 19 12	11.00	Be	..., 284	N17, DEM 59
78	52–68	269050	05 07 32.9	−68 36 00	11.54	B0Ia	202, 223	N100, DEM 76[a,b]
...	91–69	269327	05 17 48.7	−69 54 22	10.74	B0:	..., ...	...
87	95–69	269333	05 18 39.2	−69 14 45	11.21	W+B1:I	..., 271	N119, DEM 132
...	40–65	271163	05 18 43.2	−65 44 12	11.75	B3Ia	282, ...	...
...	100–69	269351	05 19 06.0	−69 35 24	11.74	B5Ia	..., ...	...
...	103–69	...	05 19 24.0	−69 42 29	12.84	B0:	..., ...	N120, DEM 134[c]
89	107–69	269382	05 19 42.0	−69 42 17	11.24	B1	..., 270	N120, DEM 134[c]
90	106–69	...	05 19 42.0	−69 41 28	12.00	WC6:	..., ...	N120, DEM 134[c]
...	86–67	...	05 22 22.3	−67 54 22	12.53	B5:?	..., ...	N44, DEM 150
100	23–71	269475	05 23 36.6	−71 45 48	11.59	B5Ia	249, 236	N198, DEM 165[a,d]
...	84–66	271234	05 24 42.0	−66 10 23	12.06	B6:Ia	..., ...	...
101	30–71	269547	05 26 55.2	−71 36 18	11.61	B5I	210, 236	Near N205B
103	82–68	269546	05 27 02.1	−68 52 17	9.88	B5I+W	..., 283	N144, DEM 199[a]
...	33a–71	...	05 29 55.7	−71 04 05	11.20	B5Ia	..., ...	N206, DEM 221[c]
...	41–71	...	05 31 20.2	−71 08 06	12.84	O-B0	..., ...	N206, DEM 221[c]
112	42–71	269660	05 31 27.4	−71 06 06	11.15	B1.5Ia	..., 222	N206, DEM 221[c]
113	45–71	269676	05 31 55.9	−71 05 49	11.47	O6e	..., 229	N206, DEM 221[c]
131	239–69	269902	05 38 29.6	−69 07 58	10.24	A0I	..., 254	N157 = 30 Dor
134	...	...	05 39 01.2	−69 07 31	...	...	..., ...	30 Dor
136	243–69	38268	05 39 02.9	−69 07 40	9.15	O+WN	..., 259	30 Dor
137	...	...	05 38 57.2	−69 06 39	...	...	..., ...	30 Dor
139	...	...	05 39 02.2	−69 06 30	...	...	..., ...	30 Dor
140	...	...	05 39 01.9	−69 06 44	...	...	..., ...	30 Dor
144	246–69	38282	05 39 13.2	−69 03 33	11.13	WN7	..., ...	30 Dor
145	248–69	269928	05 39 17.3	−69 07 38	12.02	WN6-7	..., ...	30 Dor
...	155–68	...	05 43 16.3	−68 57 54	12.72	B0.5	..., ...	N165, DEM 299[a]
				Small Magellanic cloud				
...	...	BBB 275	00^{h}46^{m}21^s.5	−73°27′35″	14.4	...	..., ...	[e]
5	27	HD 4862	00 47 16.1	−73 38 04	11.0	B3Ia	137, 141	...
...	31	Th 4[f]	00 48 00.4	−73 12 01	11.2	B2-B5Ia	159, ...	...
6	33	HD 4976	00 48 18.0	−73 24 07	11.0	B5-B7Ia	174, 157	...
8	39	HD 5030	00 48 46.7	−73 45 05	11.2	B9-A0Ia	164, 157	...
9	40	HD 5054	00 48 53.4	−73 44 41	11.1	B2-B3Ia	149, 157	...
11	56	HD 5291	00 51 19.7	−72 54 17	10.9	B8.5Ia[g]	142, 147	...
14	78	HD 5980	00 57 22.9	−72 26 36	11.8	WP+OB+Neb:	215, ...	N66B, DEM S103[h]
17	82	Arp h[i]	00 58 07.8	−73 01 08	12.1	B0-B1Ia	163, 158	...
18	85	...	00 58 26.6	−72 30 11	12.1	B1-B1.5Ia	161, 170	...
27	106	CPD−72 77	01 01 12.8	−72 26 24	10.9	B8-B9Ia	163, 132	DEM S123
36	114	Arp e[i]	01 03 12.0	−72 22 25	11.4	B3Ia	184, 185	DEM S124
37	117	Arp b[i]	01 03 15.8	−72 24 43	11.2	B6-B7Ia	189, 169	DEM S124
40	130	HD 6884	01 05 45.8	−72 44 03	10.5	B8-B9Ia	166, 170	Hα in emission
42	137	HD 7099	01 07 32.5	−72 48 20	11.0	B2-B3Ia	231, 236	...
44	...	HD 7113	01 07 43.9	−73 27 41	...	...	..., 155	...
45	152	HD 7583	01 12 07.3	−73 36 05	10.2	A0-A1Ia	171, 164	...
...	191	...	01 40 44.9	−74 05 39	11.9	OB[j]	106, ...	In SMC wing

[a] Possibly a SNR.
[b] The central star of N100, according to Feast *et al.* 1960.
[c] Definite SNR.
[d] Close to the nebulosity.
[e] From Basinski *et al.* 1967.
[f] Thackeray 1962.
[g] From Ardeberg and Maurice (1977).
[h] Possibly a SNR.
[i] Arp 1958.
[j] Sanduleak 1969.

10%, and those of the weaker features to ~15%, the error mostly arising from problems in placement of the continuum.

III. DESCRIPTION OF THE DATA

The primary purpose in obtaining these data was to provide as many lines of sight with as large a variety of angular separations as possible. Accordingly, investigation of the initial set of widely distributed stars in the Clouds (separations greater than 1°) was followed up with more detailed studies of selected regions to sample smaller separations. The final set of spectra covers angular scales from ~10″ to tens of degrees and includes some heavily sampled regions, such as 30 Doradus and the regions around the stars R112 and R89. The properties of the observed stars are given in Table 1. The following information is presented in columns (1)–(9): column (1), the Radcliffe number, according to Feast, Thackeray, and Wesselink (1960); column (2), the number from the catalogs of Sanduleak (1970) for the LMC and Sanduleak (1968, 1969) for the SMC; column (3), the number from the Henry Draper Catalog or (for the SMC) some other designation identified in the notes; columns (4) and (5), the right ascension and declination for epoch 1950.0; columns (6) and (7), the visual magnitude and spectral type, from the compilations of Rousseau *et al.* (1978) for the LMC and Azzopardi and Vigneau (1982) for the the SMC; column (8), the stellar radial velocity in the local standard of rest (LSR) frame from Feast, Thackery, and Wesselink (1960) (*left*), Fehrenbach and Duflot (1974, 1982) (*right*, LMC) or Ardeberg and Maurice (1977) (*right*, SMC); column (9), associated nebulosity from Henize (1956) (N) and Davies, Elliott, and Meaburn (1976) (DEM). The spatial coverage is illustrated in Figure 1. Figure 1*a* shows the region of the Clouds in Galactic coordinates with the positions of the observed stars and of Fairall 9, a Seyfert galaxy lying behind the Magellanic Stream that shows absorption from the Stream in Ca II (Songaila 1981*a*). Also shown schematically (*dashed lines*) are the outer extents of the globular cluster systems (Mathewson *et al.* 1979), while the shaded area is approximately the region inside the contour of H I column density equal to 4×10^{19} cm^{-2}, adapted from Mathewson, Cleary, and Murray (1974). This contour clearly shows the common H I envelope around the Clouds and its relation to the Magellanic Stream. The two straight lines are the rotation axes inferred from H I studies, taken from Mathewson *et al.* (1979). Figures 1*b* and 1*c* show enlargements of positions of stars in the LMC and SMC respectively, in equatorial coordinates. In Figure 1*b*, the shaded area is the region of complex H I emission (Rohlfs *et al.* 1984 and § III*a*), while the dashed line shows schematically the outer blue isophote of the bar region, after de

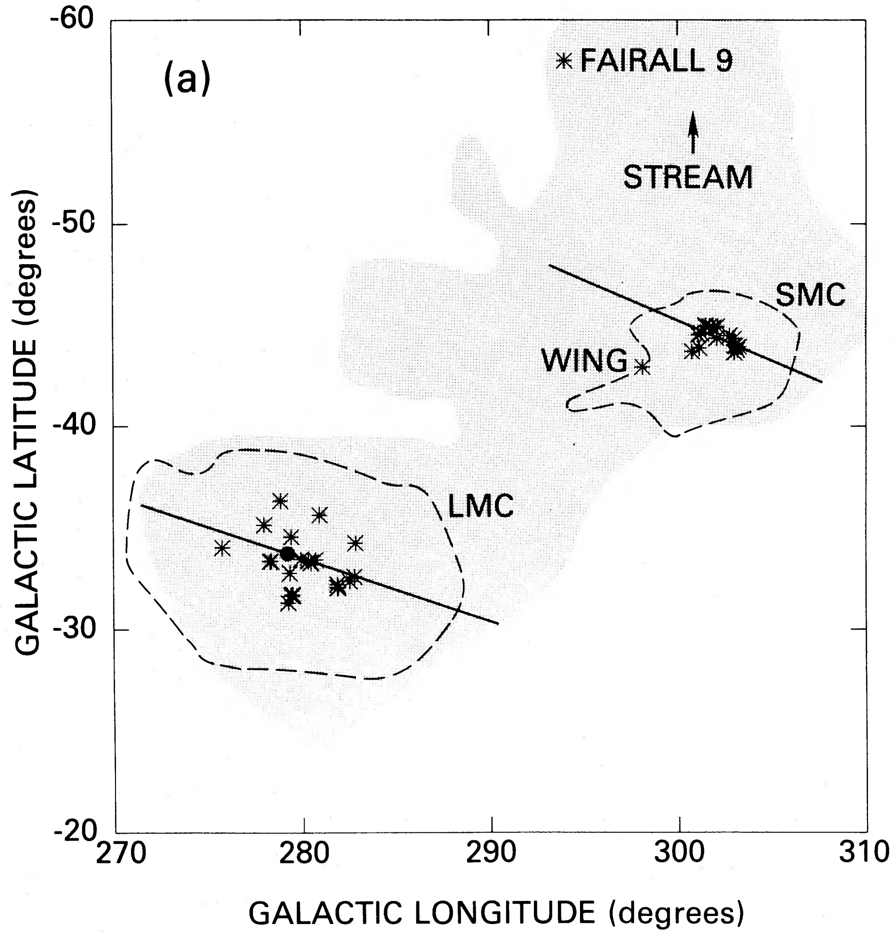

FIG. 1*a*.—Positions of observed stars within the Magellanic Clouds system. Also shown is the position of Fairall 9, where absorption from the Magellanic Stream has been observed. The shaded area is the region inside an approximate contour of 4×10^{19} cm^{-2} column density in neutral hydrogen, adapted from Mathewson, Cleary, and Murray (1974). The dashed lines show schematically the outer extents of the globular cluster systems and the solid lines the axes of symmetry, with dots at the rotation centers (adapted from Mathewson *et al.* 1979).

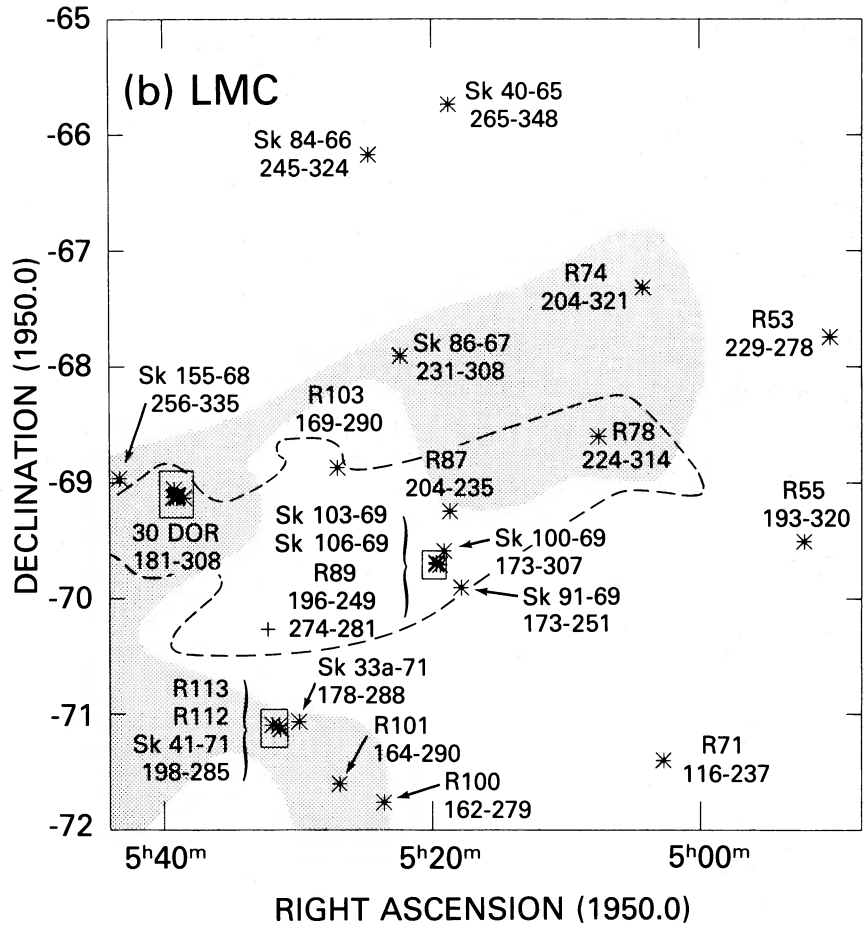

FIG. 1*b*.—Blowup of the positions of the stars within the Large Magellanic Cloud. Also shown for each star is the velocity range (in LSR) of strong calcium absorption (optical depth more than 0.1). The shading shows approximately the region of complex H I emission discussed in the text (§ III*a*), based on the data of Rohlfs *et al.* (1984), while the dashed outline is approximately the outer blue isophote of the bar region, after de Vaucouleurs (1957).

Vaucouleurs (1957). The most heavily observed regions will be described more fully later.

The typical features of spectra in the two Clouds differ enough that it is convenient to describe them individually.

a) *The Large Magellanic Cloud*

The overall features of the LMC spectra are summarized in Figure 2. Shown here are average spectra around Ca K of stars with small angular separation in each of three heavily observed regions: 30 Doradus, near R112, and near R89. The individual spectra constituting these three averages are shown in Figure 3. All the spectra are normalized to the local continuum (*dashed lines*) and are plotted against LSR velocity in the rest frame of Ca K in units of km s^{-1}.

We can use these three composite spectra to point out the principal features of lines of sight to the LMC. It is immediately obvious that all the spectra show absorption features that can be divided into four general velocity regions: near zero velocity, near $+60$ km s^{-1}, near $+120$ km s^{-1}, and greater than $+180$ km s^{-1}. Figure 4 shows a histogram of the distribution of absorption components toward the LMC and SMC. (Results for Sk 191 in the SMC wing and for Fairall 9 will be discussed later, and the significance of the horizontal bars is addressed in § IV*c*). The solid histograms refer to "strong" absorption (optical depth $\tau > 0.1$) and the dashed lines to the remaining "weak" components. It is clear that, away from the local gas, the bulk of strong calcium absorption occurs at LSR velocities between 200 and 300 km s^{-1} (GSR velocities between -6 and $+94$ km s^{-1}), while weak features spread all the way from the zero-velocity gas up to the velocity of the LMC. The distribution of components in velocity space clearly shows that the weakly absorbing gas preferentially clumps between 40 and 60 km s^{-1} and between 100 and 120 km s^{-1}. There does not appear to be any such weak interstellar absorption at velocities higher than 300 km s^{-1}, though McGee, Newton, and Morton (1983) and Rohlfs *et al.* (1984) report weak H I emission out to 360 km s^{-1} in some lines of sight.

The material near zero velocity is found in all lines of sight and is almost certainly gas in the Galactic disk. The equivalent widths (200 mÅ) and velocities (0–10 km s^{-1}) are quite typical of other long paths out through the Galaxy (Greenstein 1968; Blades and Morton 1983). This paper will not address the local absorption further, although these data could be of considerable interest for investigating the small-scale structure of the local interstellar medium; the smallest angular separation of the observed stars corresponds to $\sim 10^{15}$ cm tranverse scale at a distance of 100 pc.

Turning next to the strongly absorbing gas ($\tau > 0.1$), Figures 2 and 3 demonstrate that most of the stars show several quite distinct components. Thus, for example, in the R89 region, there are components at LSR velocities of 210, 235 and

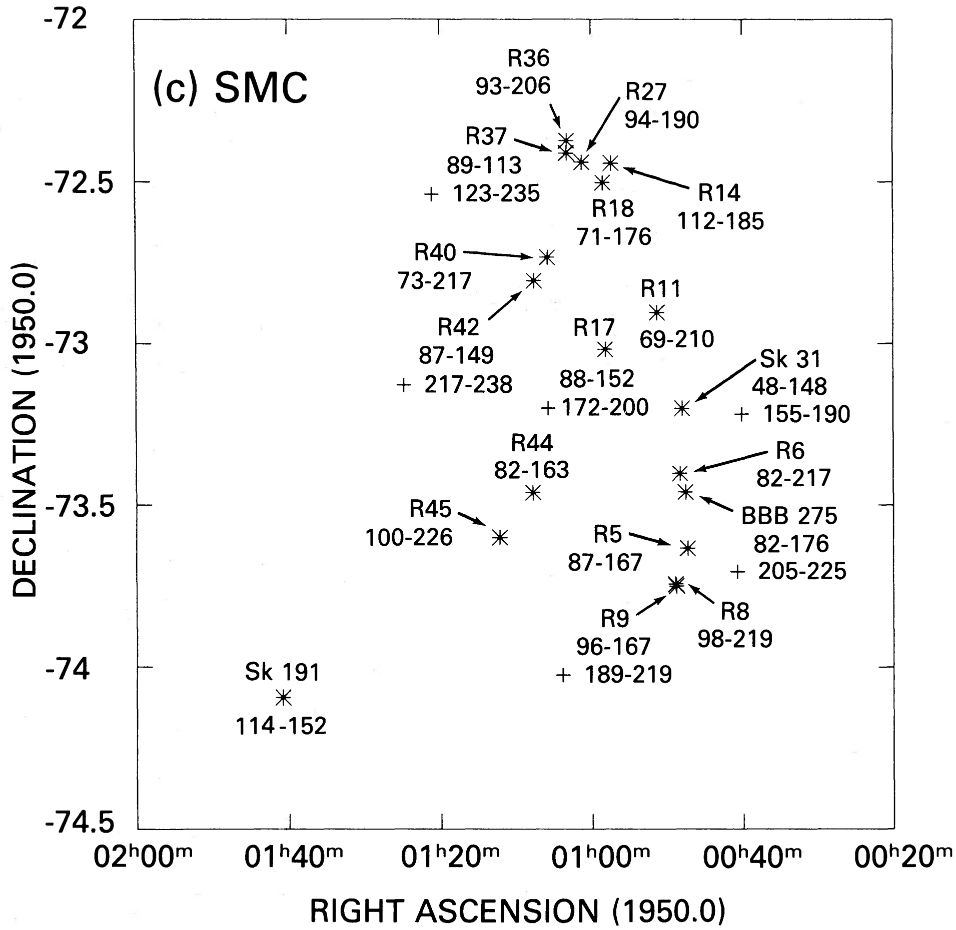

FIG. 1*c*.—Blowup of the positions of the stars within the Small Magellanic Cloud. Again the velocity range of strong absorption is shown.

280 km s^{-1} with relative strengths varying considerably from star to star, while in the R112 region, absorption occurs between 210 and 280 km s^{-1}, although with a somewhat smoother distribution and with the 280 km s^{-1} component being very weak. We have summarized in Figure 1*b* the velocity range over which strong absorption occurs in each star.

From recent measurements, Rohlfs *et al.* (1984) have suggested that neutral hydrogen within the LMC appears primarily to be in the form of a shearing sheet of gas with a rotation axis at 28° east of north, a central velocity of 260 km s^{-1} LSR, and projected rotation velocity of about 25 km s^{-1}; the highest velocity material lies in the northeast. This structure can also be seen in the calcium data of Figure 1*b*. As can be seen from Figure 5 of Mathewson *et al.* (1979), this velocity structure smoothly connects through gas in the inter-Cloud region onto the material at the position of the SMC and should probably not be interpreted as simple rotation in the field of the LMC. In addition, throughout much of the LMC, the velocity structure is more complicated, containing several neutral hydrogen peaks. The complex regions are shown schematically in Figure 1*b*. They stretch up from R112 through 30 Doradus and then bend through the bar region around R87 and finally up to R74. Feitzinger (1980), Feitzinger and Schmidt-Kaler (1982), and Rohlfs *et al.* (1984) suggest that this complex structure is caused by a spatially separate region of gas being seen in projection against the primary material. From McGee and Milton's (1966*b*) discussion, roughly a third of the $5.4 \times 10^8 \, M_\odot$ of neutral hydrogen lies in this region.

We can use the calcium absorption data to investigate whether there are in fact two spatially separate regions along this line of sight by looking for systematic differences between calcium seen in projection in front of the stars and neutral hydrogen profiles where we integrate through the entire LMC. The comparison of neutral hydrogen with strong calcium absorption along individual lines of sight is presented in Figure 5, where the velocity extents of Ca K absorption are shown as vertical lines superimposed on contour plots of relative intensity of H I emission, taken from McGee and Milton (1966*a*). Only the contours of 2.5 (*dotted*), 5, 10, and 15 units are shown (1 unit = 1.75 K of brightness temperature T_b). The vertical axis is heliocentric radial velocity, and the declination of each velocity–right ascension cut is shown in the upper right corner of each panel. The strong calcium absorption is slightly more sensitive than the early neutral hydrogen surveys, and along most lines of sight the Ca K velocity width is similar to or larger than that of the hydrogen. This somewhat surprising result suggests that most of the observed stars lie toward the rear of the Cloud behind the bulk of the gas. However, in a number of lines of sight (e.g., toward R71, R87, R89, Sk 91–69, and Sk 155–68), material is present in neutral hydrogen which is not seen in calcium absorption. Thus the gas at about 250 km s^{-1} LSR appears to lie behind the material at lower

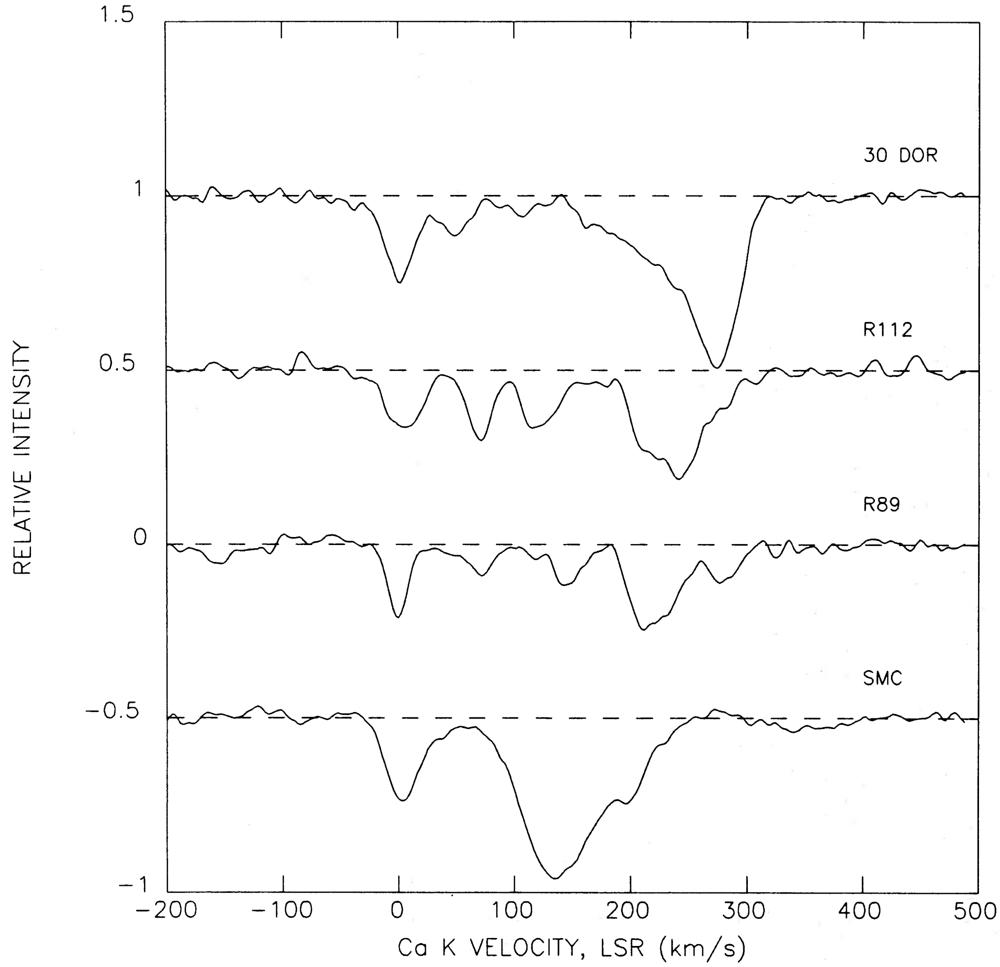

FIG. 2.—Composite spectra near Ca K λ3933.663 of three heavily observed regions within the LMC. Each spectrum is the three-point smoothed average of spectra of a number of stars in the region designated. See the text and Fig. 3 for details of the exact composition of the spectra. Each spectrum has been normalized to a polynomial continuum fitted to neighboring points (*dashed line*) and plotted against LSR velocity in the rest frame of Ca K. (Thus the dashed lines are at unit intensity, and the zero point for each spectrum is one intensity unit lower.) The bottom panel shows for comparison a composite spectrum that is the average of spectra of 16 stars in the SMC.

and higher velocities, and Feitzinger's suggestion that there are two spatially separate regions appears correct. Since some stars do show all the neutral hydrogen components, there must be early-type stars in both foreground and background material.

The overall structure is shown in a slightly different way in Figure 6, where we present the velocity widths of the K line in the stars ordered along the axis of rotation of the main neutral hydrogen feature (Rohlfs *et al.* 1984). Dashed lines refer to stars projected onto the region of multiple H I emission peaks (Fig. 1*b* and Rohlfs *et al.* 1984). The systematic trend in velocity identified by Rohlfs *et al.* is clear, though many lines of sight show material in forbidden velocity regions. We have also marked stellar velocities where known. Unfortunately, there is no clear pattern of behavior for the early-type supergiant velocities, and, in particular, we are not able to distinguish stars in the foreground or background gas on this basis.

We turn finally to the weak absorption features, which are an extremely interesting aspect of the spectra and were the intital impetus for this study. These features correspond to those first seen in UV spectra of Magellanic Cloud supergiants by Savage and de Boer (1979, 1981) and assumed by them to arise in absorption by interstellar clouds situated in a supposed gaseous halo of the Galaxy. They were subsequently seen in optical absorption spectra of the present type (Songaila and York 1980; Blades 1980) and in weak neutral hydrogen emission (McGee, Newton, and Morton 1983). By assuming a simple corotating model of this halo, Savage and de Boer estimated that these clouds lie ~10 kpc below the Galactic disk. Assuming that this was true, and that the clouds are condensations at 10^4 K in a hot corona, Songaila (1981*b*) found that reasonable constraints could be placed on the density and temperature of such a corona. However, York (1982) has argued that the Magellanic Cloud lines of sight are unusually rich in absorption features compared to other lines of sight out through the halo of the Galaxy, and this suggests that the features may be produced by the Clouds themselves.

One of the principal functions of this work is to reexamine the case for the halo origin of these features, using this much larger set of data, which covers a greater sample of scale sizes than has been available before. Although the clearest conclusions will arise from the SMC data, several points can be made immediately from the LMC data. First, it is clear that this absorption is a feature of the LMC line of sight as a whole and

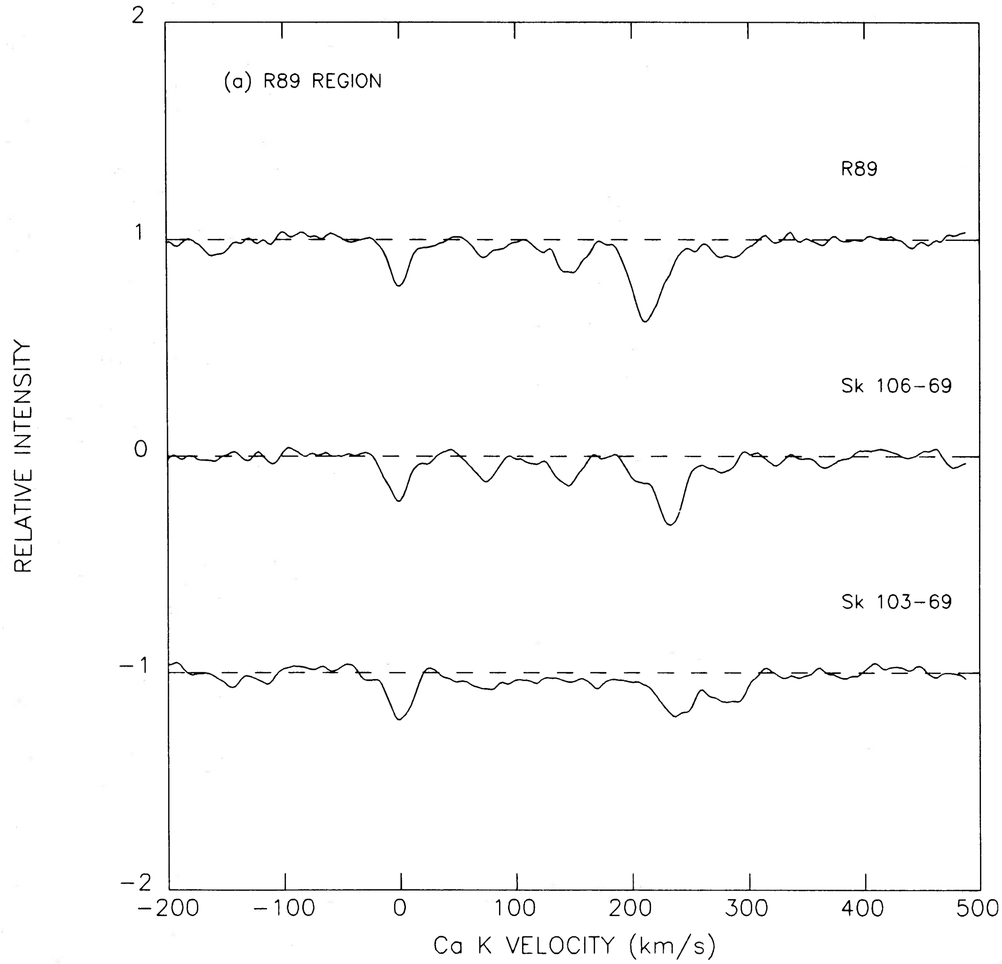

FIG. 3*a*.—Spectra at Calcium K of stars in the neighborhood of R89 in the LMC. These are the spectra constituting the average spectrum labeled "R89" in Fig. 2. The spectra are smoothed and normalized as described in Fig. 2 and the text. (*b*) Same for the region around R112 in the LMC. (*c*) Same for stars in the line of sight to the 30 Doradus nebula.

that the features are not produced by individual events within the LMC or the Galaxy. The presence of the features over much of the face of the Cloud shows that they are either truly a phenomenon in the halo of our Galaxy, unconnected with but covering the LMC, or that they are in some way a global phenomenon of the LMC. The ubiquitous nature of the features shows that, although the implied gas velocities (~ 100 km s^{-1} relative to the LMC) are quite typical of velocities in supernova remnants, and many of the stars lie in or near nebulosity, this cannot be the explanation of the weak absorption. Similarly, any connection of the weak absorption features with shells of gas around associations in the Cloud seems to be ruled out by this data set. The 30 Doradus composite profile (Fig. 2) and individual profiles (Fig. 3*c*) make this quite clear. The composite profile tends to average out the structure in the extended blueward wing that is seen in individual profiles, but it does, on the other hand, quite clearly limit the velocity extent of this wing to $+150$ km s^{-1}. Furthermore, two completely separate weak absorption features are also strongly present in the profile. This very strongly suggests that the weak absorption features are not connected with individual events in the LMC.

It is much more difficult on the basis of the LMC data to decide definitely between a halo origin of the features and some model which places the absorption closer to or within the Clouds. However, Figure 2 does unambiguously show that it is impossible to find distances to the absorbing clouds by using a simple corotating halo model: since the components shift substantially in velocity among the three profiles, it is clear that they cannot arise in quiescent clouds with single velocities from which a distance can be assigned. We can also argue that the distance scale over which substantial variation in individual profiles occurs would tend to shift these absorption features closer to the LMC. For example, in Figures 3*a* and 3*c*, the features are stable over a separation of $10''$–$\sim 30''$ but vary substantially when the separation rises beyond this. At the distance of the LMC, this implies uniformity over a distance of several parsecs (roughly the scale size of "standard" clouds in our own interstellar medium), but in a halo at 10 kpc from the Sun, the scale size for variation becomes very small ($\ll 1$ pc). This argument is of course quite weak, since we do not properly understand scale sizes in our own interstellar medium, let alone in the Galactic halo or in irregular galaxies. However, Cohen (1981, and earlier papers cited therein) does find uniformity on scale of a few arcminutes for interstellar absorption features seen against globular cluster stars. We might also emphasize the apparent uniqueness of the complexity of weak absorption material observed in this line of sight compared to

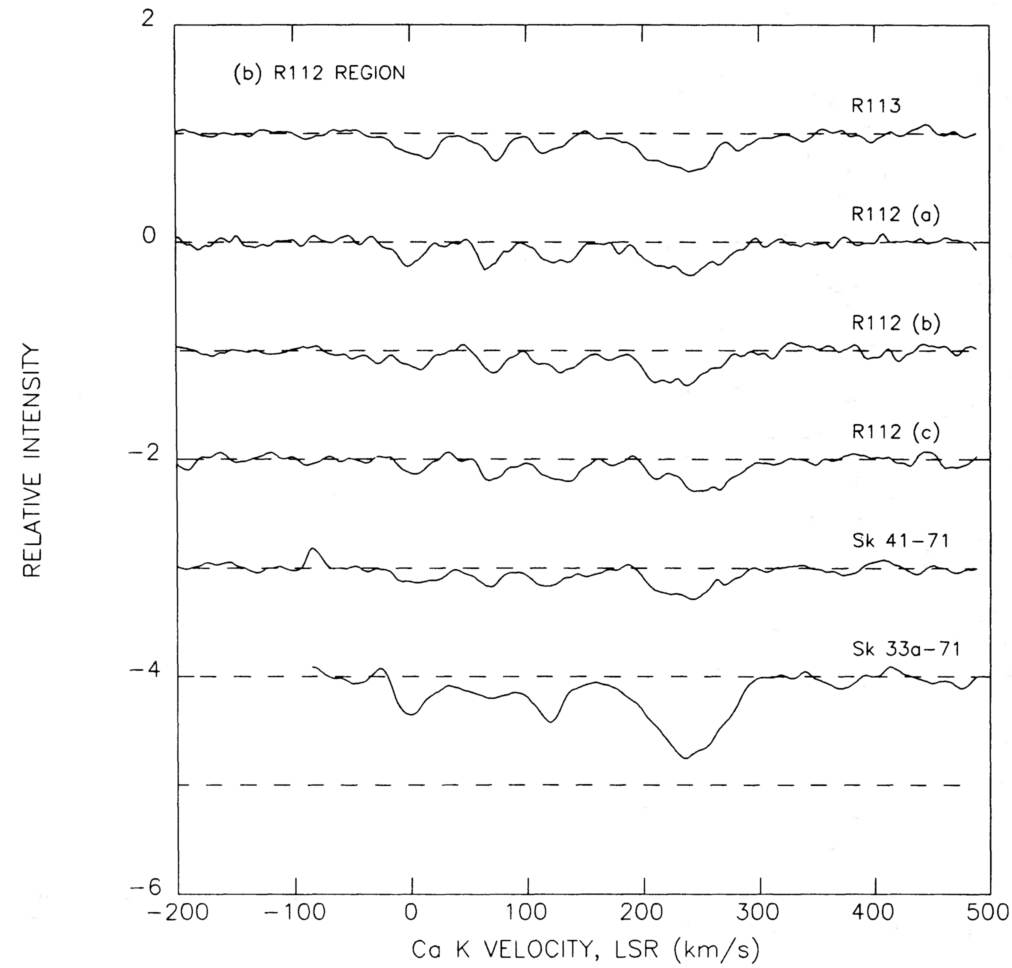

FIG. 3b

other lines of sight through the Galactic halo. (See York 1982 for a general discussion of the properties of absorption observed in other long paths through the Galaxy.)

b) Small Magellanic Cloud

The spectra around Ca K of stars in the SMC that have not previously been published are shown in Figure 7. These spectra have been flattened and smoothed as described in § II and are plotted in LSR velocity. Figure 8 gives the corresponding comparison of Ca K absorption with neighbouring H I emission profiles from the survey of McGee and Newton (1982*a*, *b*). From this figure we can see that the general structure of gas in this region is similar to that in the LMC, though there are considerable differences in detail. One similarity is the presence in these spectra of weak absorption at velocities outside the normal limits of Galactic or SMC absorption. For example, in the spectra of R27, R14, and R18 there is absorption between 30 and 90 km s^{-1} that has no counterpart in the H I profile in this direction. In some stars, for example R36, the higher velocity part of this material (above 50 km s^{-1}) is missing, but in general almost all lines of sight show some material between 30 and 90 km s^{-1} with column density a few times 10^{11} cm^{-2} in Ca II, similar to the strength of corresponding material toward the LMC. However, a striking difference between the two Clouds is that, in some SMC lines of sight, these weak features extend *beyond* the velocity of the main bulk of the SMC gas as outlined in the H I profiles. This is seen, for example, in the spectra of R36 and R37 which show weak features out to ~260 km s^{-1}, with no corresponding H I. Another similar example is the spectra of R8 and R9. Both these examples are important, in that they eliminate the worrying possibility that most of this absorption might be coming from stellar line contributions from stars that are generally of somewhat later type (B3–B9) than the sample in the LMC. In both cases, the pairs of stars are close to one another on the sky and have quite different spectral types. It is clear that the star of later type in each case has extra absorption at the stellar velocity, but in both cases this is well away from (≥ 50 km s^{-1}) the weak high-velocity absorption in question. This extension of weak absorption beyond the velocity of the SMC is seen more globally in Figure 4, where it is compared with the LMC.

An interesting morphological structure emerges when the strongly absorbing material is studied (see also Cohen 1984). Figure 8 shows that the neutral hydrogen has two clearly defined peaks at ~120 km s^{-1} and ~165 km s^{-1} (LSR) with relative intensities that vary with position in the Clouds. In general, the higher velocity component is relatively stronger toward the northwest of the SMC, the components are about equally strong towards the center (R11, R17, R6), and the lower velocity component is stronger to the southwest. As Mathewson and Ford (1984) discuss in detail, this is readily explained by the superposition of two dense sheets of gas of varying

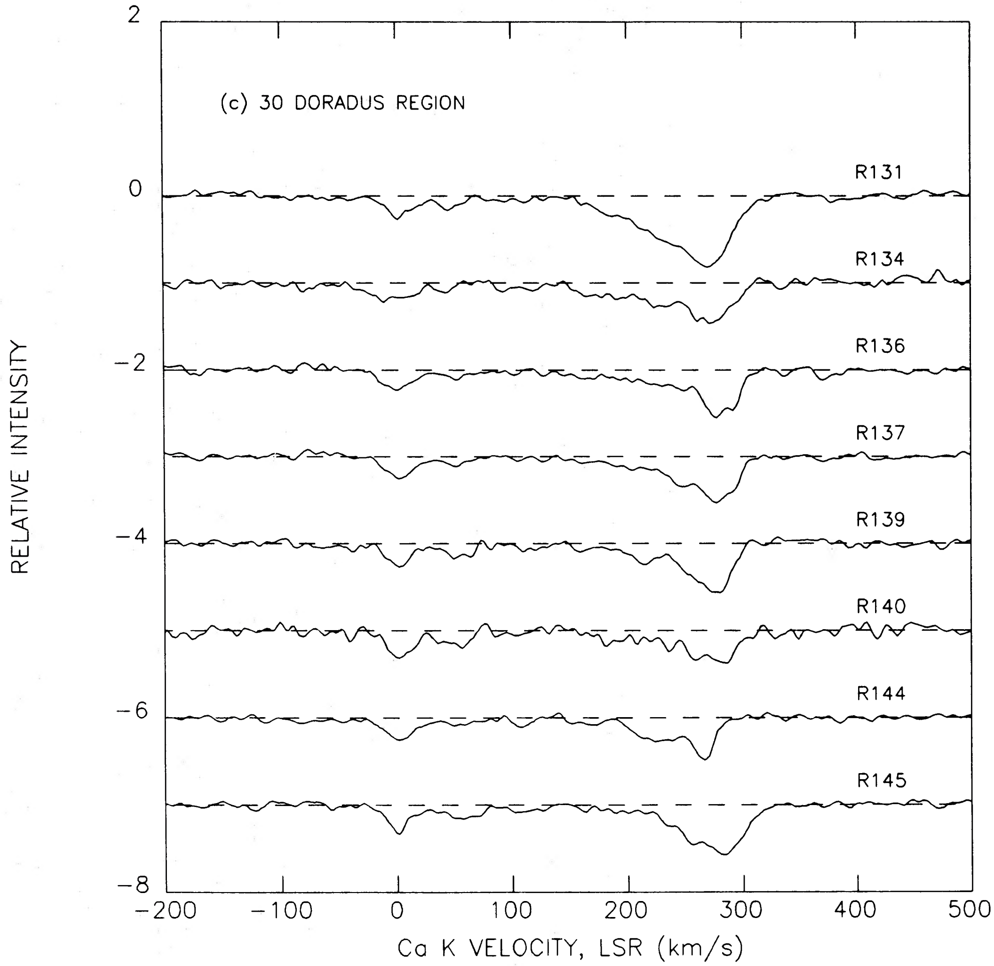

FIG. 3c

column density which are spatially and kinematically separated. There is, of course, no way of knowing anything about the spatial separations of these sheets from the H I information alone, but a study of the corresponding calcium absorption lines is very revealing. Basically, the calcium profiles split into three classes: (*a*) those with absorption only between 120 and 140 km s^{-1}; (*b*) those with strong absorption at $\sim$120 km s^{-1} accompanied by weak absorption between 200 and 240 km s^{-1}; and (*c*) those with strong absorption at $\sim$120 km s^{-1} and $\sim$165 km s^{-1} and weak absorption at 200–240 km s^{-1}. No other combinations are seen in these profiles, although a few spectra are complicated by unfortunately strong stellar lines.

Turning first to category (*c*), good examples are the spectra of R36, R37, and R11 and possibly those of R5 and R9, although in these last the absorption near 165 km s^{-1} might be stellar, placing those spectra in category (*b*). R14 probably also lies in this category. It is clear that, in all cases, there is less absorption near 165 km s^{-1}, relative to that at 120 km s^{-1}, than the corresponding H I column densities would imply. Taken together with the fact that *all* lines of sight show absorption near 120 km s^{-1}, this implies that the higher velocity H I sheet is at a greater distance and that the stars that show this absorption are embedded within this sheet to varying extents.

Good examples of category (*b*) are possibly the spectra of R5 and R9, as mentioned, and also those of R6, R17, BBB275, and R42. The most unambiguous cases are those of R17 and R42, where there is no absorption near 165 km s^{-1} even including, for R17, any stellar contributions. The high-velocity (240 km s^{-1}) material in the R42 spectrum could be contaminated by a stellar contribution from this B2–3 Ia star. The BBB 275 spectrum has no convincing component at 165 km s^{-1} above the noise. Finally, the spectra of R5, R9, and R6 are ambiguous, the small contribution at 165 km s^{-1} possibly being stellar in each case. The important fact to note is that all these spectra that lack absorption at 165 km s^{-1} have absorption at 120 km s^{-1}, implying that the stars lie between the two H I planes. Also, all spectra show absorption near 220 km s^{-1}, showing that this material is also in front of the H I plane at +165 km s^{-1}. Moreover, because there are spectra in category (*a*) that show absorption only near 120 km s^{-1}, and none at either high velocity, the weakly absorbing material at 220 km s^{-1} must be sandwiched between the main layers.

The best examples of category (*a*) spectra are those of R44, R18, Sk 31, and Sk 191. In all these cases, higher velocity absorption is definitely absent. A slightly puzzling detail is that the main absorption in the R44 and R18 spectra is slightly to the red of the corresponding H I emission. This could be explained by a redward shift in the center of gravity of the absorption caused by blending with the stellar line. Finally, we note that we have excluded the spectra of R8, R27, R40, and

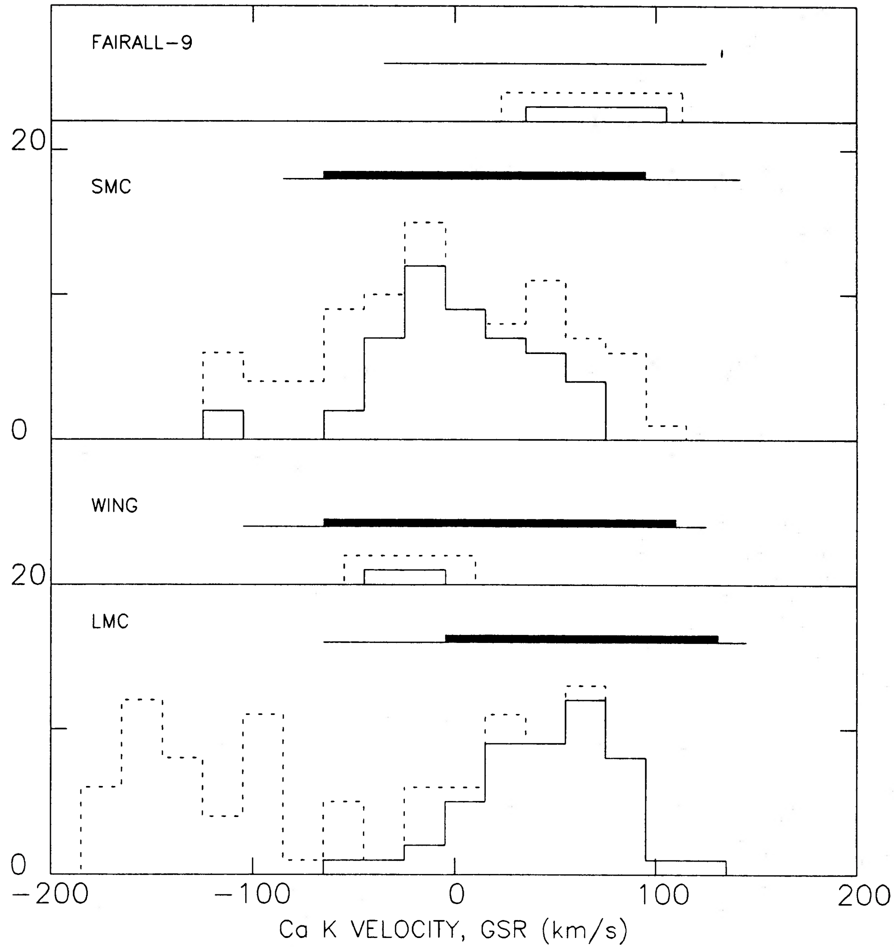

FIG. 4.—The distribution of absorption components with velocity for stars in the LMC, Sk 191 in the wing of the SMC, the remaining stars in the SMC, and the Seyfert galaxy Fairall 9 which lies behind the Magellanic Stream (Songaila 1981*a*). The solid lines refer to "strong" components (optical depth greater than 0.1) and the dashed lines to the remaining "weak" components. For Sk 191 and Fairall 9, the solid line gives the velocity extent of "strong" absorption, and the dashed line the full extent of a single absorption line in each case. The velocity scale has been corrected for a solar motion of 20 km s^{-1} with respect to the LSR and 250 km s^{-1} about the Galactic center. The horizontal bars above each histogram are the expected extents in radial velocity for particles in each of these directions according to the best-fit model of Murai and Fujimoto (1980), adapted from Fig. 8*c* of that paper. The solid line refers to the extent of the bulk of the particles, while the dotted line shows the complete velocity range for all particles.

R45, whch are late B-type and hopelessly contaminated by stellar lines.

These results for the SMC are consistent with those of Cohen (1984), who concluded that the high-velocity H I lies behind the lower velocity material. However, she did not discuss the weakly absorbing very high velocity gas, presumably not detected in her much lower resolution (55 km s^{-1}) spectra. In addition, unlike Cohen, we do not see a strong tendency for the calcium absorption to be at the lower H I velocity only.

This distance ordering by velocity structure is fairly consistent with distance moduli give by Ardeberg and Maurice (1979). The average of the distance moduli of R36, R37, and R11 is 18.86; of R5 and R9 is 18.76; and of R6 and R42 is 18.63. Unfortunately, moduli for R17 and BBB275 are not available, while Sk 31 is the only star of category (*a*) which was measured by Ardeberg and Maurice; it was found to have a distance modulus of 18.73. Omitting category (*a*), therefore, this is still roughly consistent with a difference in distance modulus of ~ 0.25 mag between stars in categories (*b*) and (*c*). That is, the distance between the main "sheets" of H I would be at least 10 kpc. Distance moduli for the remaining stars would be very desirable, particularly those of the "front" plane, to see if this highly tentative result holds up.

In contrast with this relative regularity, the stellar radial velocities, like those of the LMC, are much more confused. This is illustrated in Figure 9. The velocities are those of Ardeberg and Maurice (1977), or from Feast, Thackeray, and Wesselink (1960) if no Ardeberg and Maurice measurement is available, corrected for motion of the Sun with respect to the LSR (20 km s^{-1}) and the Galactic center (250 km s^{-1}). The outer histogram is the distribution of Ardeberg and Maurice's (1979) sample of 52 early-type stars. Within this is our sample of 18 supergiants, split into four groups corresponding to stars from categories (*a*), (*b*), and (*c*) above (see § III) and those remaining unclassified. As in the LMC, the stellar radial velocity does not give a clear measure of position within the SMC.

IV. DISCUSSION

a) *The Origin of the Weak Absorption Features*

On the basis of the present results, it seems quite unambiguous that there exist within the LMC and SMC planes of

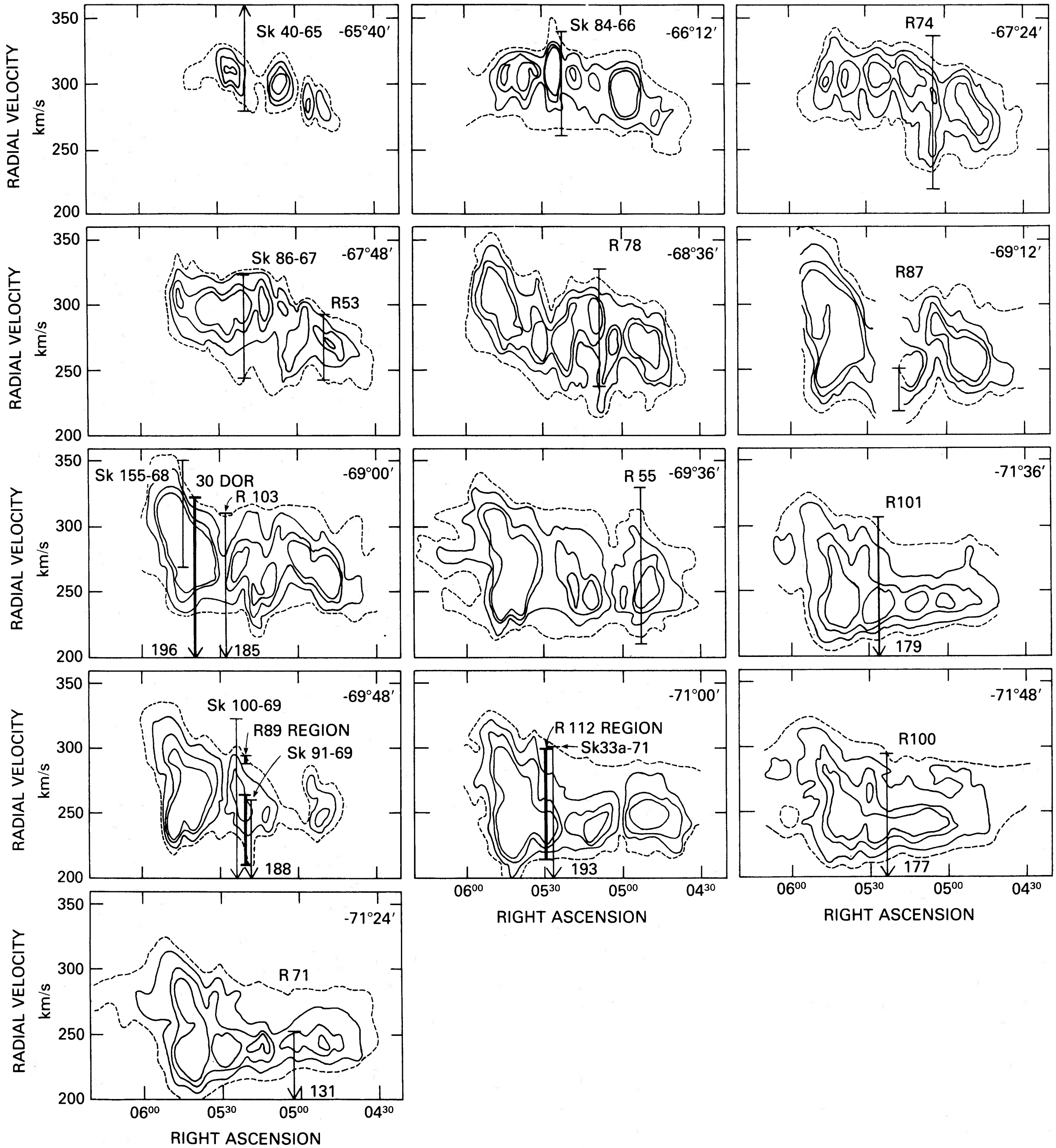

FIG. 5.—Comparison between the velocities of H I emission and Ca K absorption for individual stars in the LMC. The contour plots of relative intensity of H I emission are adapted from McGee and Milton (1966*a*). Only the contours of 2.5 (*dotted*), 5, 10, and 15 units are shown (1 unit = 1.75 K of T_b). The vertical axis is heliocentric radial velocity, and the declination of each velocity–right ascension cut is shown in the upper right corner of each panel. Superposed on these contours are vertical lines denoting the velocity extents of strong ($\tau \geq 0.1$) Ca K absorption in the labeled stars.

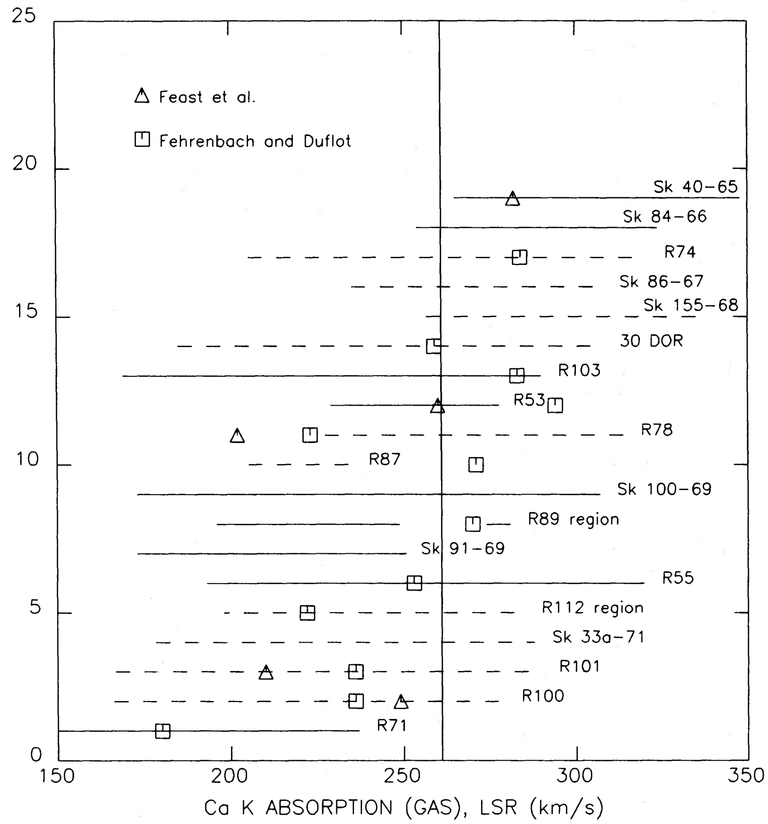

FIG. 6.—A summary of Ca K absorption velocities and stellar radial velocities for the stars in the LMC in our sample. The abscissa is radial velocity in the frame of Ca K corrected to the LSR. Each horizontal line shows the extent of strong ($\tau \geq 0.1$) Ca K absorption toward the designated star or region of stars (see Figs. 2 and 3). The stars are arranged vertically in order of their projection onto the rotation curve of Rohlfs *et al.* (1984) (see Fig. 1*a*) with stars to the northeast at the top (the ordinate is a running ordinal number), and the vertical line gives the central velocity of the H I, also according to Rohlfs *et al.* A dashed line means that a star is projected onto the region of confused H I profiles (see Fig. 1*b*) and Rohlfs *et al.* 1984). The symbols show the measured stellar radial velocities from Feast, Thackeray, and Wesselink (1960; *triangles*) or Fehrenbach and Duflot (1974, 1982; *squares*).

low column density gas which have varying velocities and each of which covers a substantial fraction of the galaxy surface. It is also clear that these features are not caused by individual events within the Clouds. If we accept that these features are a generic class, and that different components do not have different origins, as seems probable in view of their substantial similarity, then we must also conclude that they are *not* a halo component. The arguments for this are as follows: (1) we have unambiguously identified a distance to the weakly absorbing 220 km s^{-1} feature in the SMC which places it within the Magellanic Clouds; (2) features are found over a wide velocity range only some of which would be consistent with a halo origin (see Fig. 4); and (3) scale sizes of 30″ within the features correspond to natural sizes of several parsecs at the distance of the Clouds.

In spatial and velocity morphology, the weak absorption features are quite similar to the much higher column density gas which constitutes the bulk of the Magellanic Cloud gas, and it appears most likely that they are a low column density analog with a wider velocity spread. We shall discuss the origin of both features in § IV*c*.

b) The Internal Structure of the Clouds

Both the LMC and the SMC contain several distinct features of widely differing velocity and column density, which are seen simultaneously as quite discrete components at a given position and which are suggestive of individual sheets layered over one another. The spread in velocities for this material is very large, and for the highest column density features can be as much as 100 km s^{-1}. If weaker features are included, the spreads are 200–300 km s^{-1}. It should be emphasized that many of the weaker features and possibly even the strong planes may be gravitationally unbound with respect to each other (Mathewson and Ford 1984).

As we discuss below, we think that the likeliest explanation for the formation of this structure is the tidal interaction between the Clouds that formed the Magellanic Stream. Mathewson and Ford (1984) have pushed furthest in this interpretation in claiming that the SMC has broken into two components, the Mini Magellanic Cloud and the Small Magellanic Cloud Remnant. The present data suggest that this interpretation may not go far enough, and that there may be several major, and a large number of minor, fragments in the LMC and SMC which are quite spatially and kinematically distinct.

c) The Origin of the Planes in the Magellanic Cloud System

Since the discovery of the Magellanic Stream, a number of papers have discussed the origin of this prominent gas feature in terms of a tidal interaction between the Magellanic Clouds and the Galaxy. One of these, by Murai and Fujimoto (1980) (see also Lin and Lynden-Bell 1982), reproduces the details of the Stream very successfully and is the first model to treat the LMC and SMC separately. The extra freedom in this more realistic treatment of the two Clouds leads to important differ-

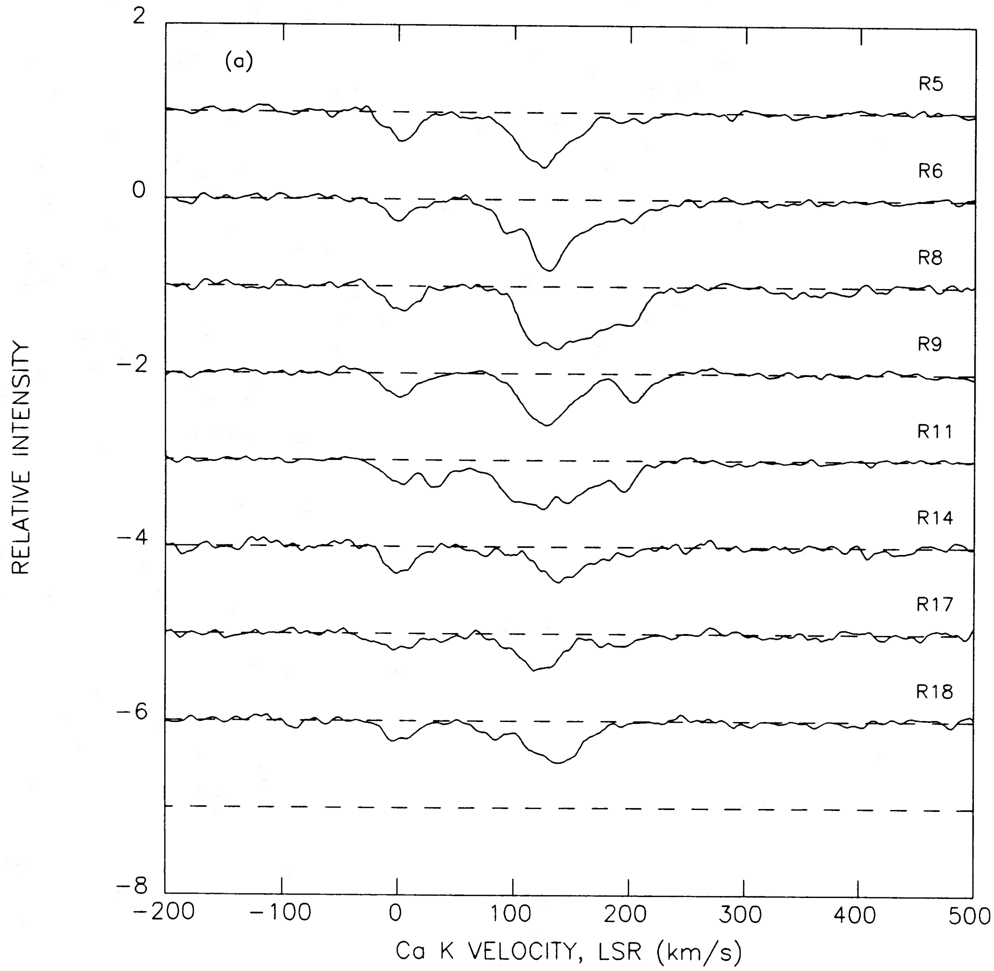

FIG. 7a

FIG. 7.—Previously unpublished spectra around Ca K λ3933.663 of stars observed in the SMC. Each spectrum is smoothed by a three-point filter and normalized to a polynomial continuum fitted to neighboring points (*dashed line*). The zero point for each spectrum is therefore the continuum of the one below. The horizontal scale is velocity in the rest frame of Ca K, corrected to the local standard of rest.

ences with the results of previous models. Most significantly, the condition that the two Clouds should have formed a bound system for the last 10^{10} yr severly constrains the possible orbits of the Clouds round the Galaxy; in particular, no orbit with perigalacticon less than 40 kpc was found to be acceptable. Therefore, in contrast with previous models (Lin and Lynden-Bell 1977), the Stream is not formed by tidal stripping from the Clouds during a close passage to the Galaxy, but rather is a product of the interaction of the LMC and SMC as separate systems. Moreover, it was found that the details of the Stream could be reproduced only by binding particles to the LMC out to a distance of 10 kpc while the corresponding radius for the SMC was only 3 kpc. Thus, in this model, the Stream is formed specifically by material torn out of the SMC by a recent (2×10^8 yr ago) close passage of the SMC to the LMC. As Murai and Fujimoto observe, this result accords well with the apparent continuity of the southern end of the Stream with the gaseous envelope of the SMC, as shown in the H I maps of Mathewson, Cleary, and Murray (1974) (see Fig. 1*a*). In addition, the material of the counterstream is largely captured onto the LMC and is not expected to be a separate feature on the sky.

One definite (and obvious) consequence of the formation of the Magellanic Stream by tidal disruption of the Clouds is that material along the line of sight to the Clouds is very likely to be widely disturbed in position and velocity, regardless of the precise nature of the interaction. In light of the discussion above concerning the complicated spatial and velocity-space structure of the gas in and near the Clouds, it seems worthwhile to compare the conclusions of these absorption-line measurements with the predictions of dynamical models. We have chosen for comparison the model of Murai and Fujimoto described above because of its more realistic individual treatment of the two Clouds; is is clear from our results that the lines of sight to the two Clouds differ in detail and can be separately compared with the model.

The comparison is summarized in Figure 4. The histograms show the distribution of absorption components with velocity toward the LMC and SMC, as has already been discussed in § III. For completeness, the results for Sk 191 in the SMC wing (this paper) and for the Seyfert galaxy Fairall 9 lying behind the Magellanic Stream (Songaila 1981*a*) are also included. In these cases, the solid line is the velocity extent of strong absorption (optical depth ≥ 0.1) in the single absorption line present, while the dotted line indicates the velocity extent of the entire line. The velocity scale has been corrected for a solar motion of

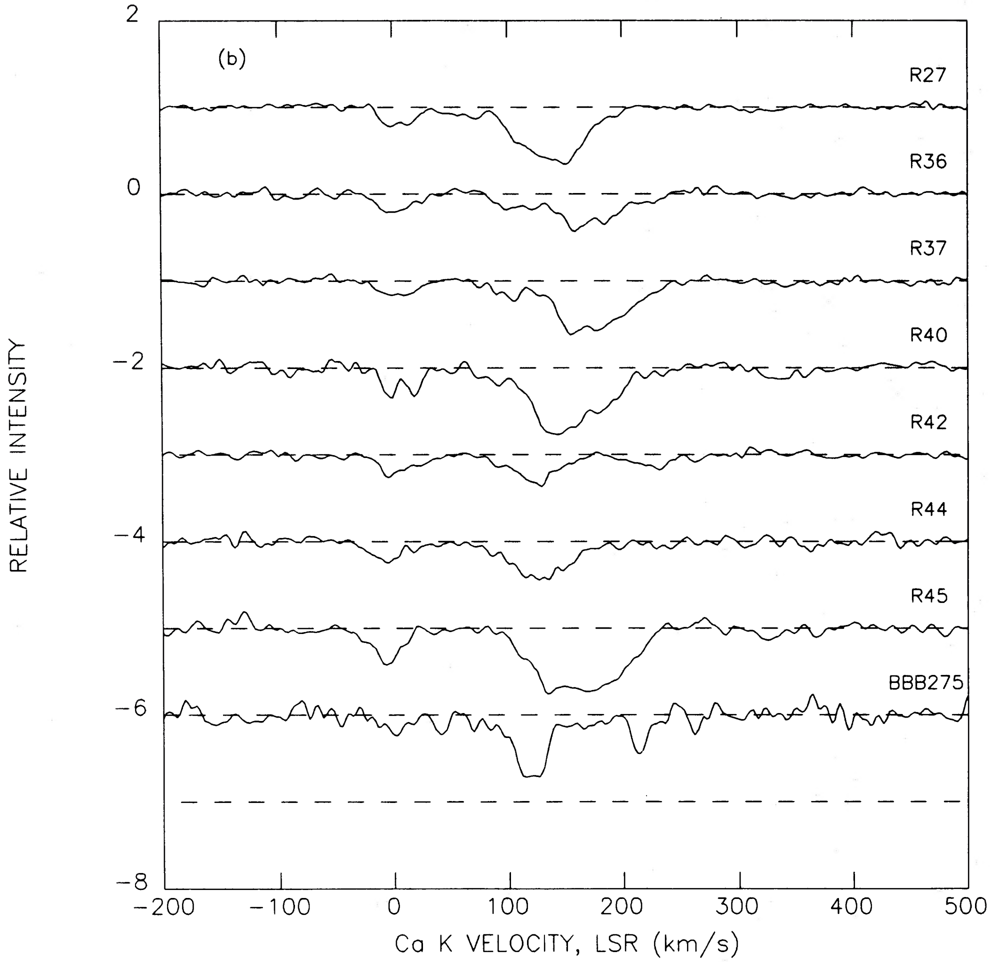

FIG. 7b

20 km s^{-1} about the LSR and 250 km s^{-1} about the center of the Galaxy. The horizontal bars above each histogram are the expected extents in radial velocity for particles in each of these directions, adapted from Figure 8c of Murai and Fujimoto. Here the solid part of the line refers to the extent of the bulk of particles, while the dotted line shows the complete velocity range.

It is interesting to note that not only is there very good agreement in general between the model and the absorption line results, but also that subtle differences among the lines of sight are also well represented in the models (at least qualitatively). For both the LMC and the SMC there is very good agreement between the model and the observations for strong absorption in the main body of the Clouds. In addition, the suggestion, from the model, of extended absorption toward higher velocities in the SMC and lower velocities in the LMC is in encouraging agreement with the absorption line results. It is also clear that the range of model velocities covers at least some of the intermediate velocity features toward the SMC. The spread to lower velocities is not so extensive for the LMC, but it should be remembered that the Murai and Fujimoto model constrained particles to be strongly bound to the LMC, so perhaps this is not too surprising.

As a final conclusion of this paper, we note that the velocity extent of gas within the LMC and SMC will inevitably result in large distance spreads of material within the Clouds. A relative velocity of 100 km s^{-1} lasting for 2×10^8 yr (the time since tidal interaction according to Murai and Fujimoto) would result in a distance spread of 20 kpc, or a range in distance modulus of around 1 mag. If the concept of fragments suggested above is correct and there is some variation in the stellar and gaseous populations of the fragments, spreads in measured distance moduli and differences between different average distance moduli may be readily understood in terms of different weightings. In particular peculiar distances to individual objects such as SMC X-1 (e.g., Howarth 1982) may simply reflect their positions within a system that is substantially extended along the line of sight.

We would like to thank Sarah Stevens-Rayburn for extensive bibliographic assistance, Mike Fall for comments on an early draft, and Don York, who initiated a large part of this project and provided encouragement at later stages. This work was supported in part by NASA Headquarters grants NAGW 208 and NAGW 464, and by a grant from the Alfred P. Sloan Foundation.

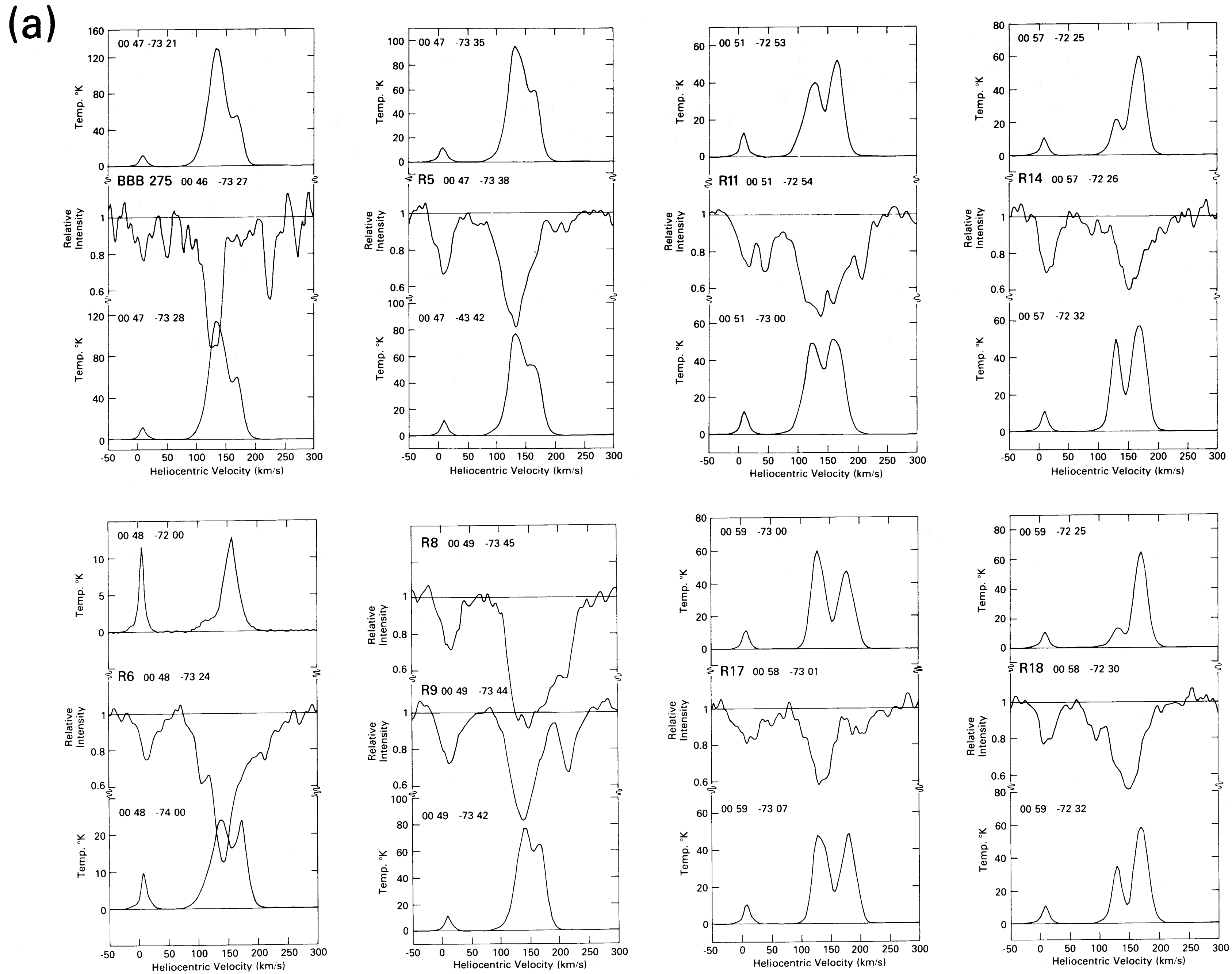

FIG. 8.—Comparison between the velocities of H I emission and Ca K absorption for individual stars in the SMC. Each absorption spectrum is bracketed by one or two of the closest H I profiles in the compilation of McGee and Newton (1982*b*). The R. A. and Decl. of each star and H I profile are given.

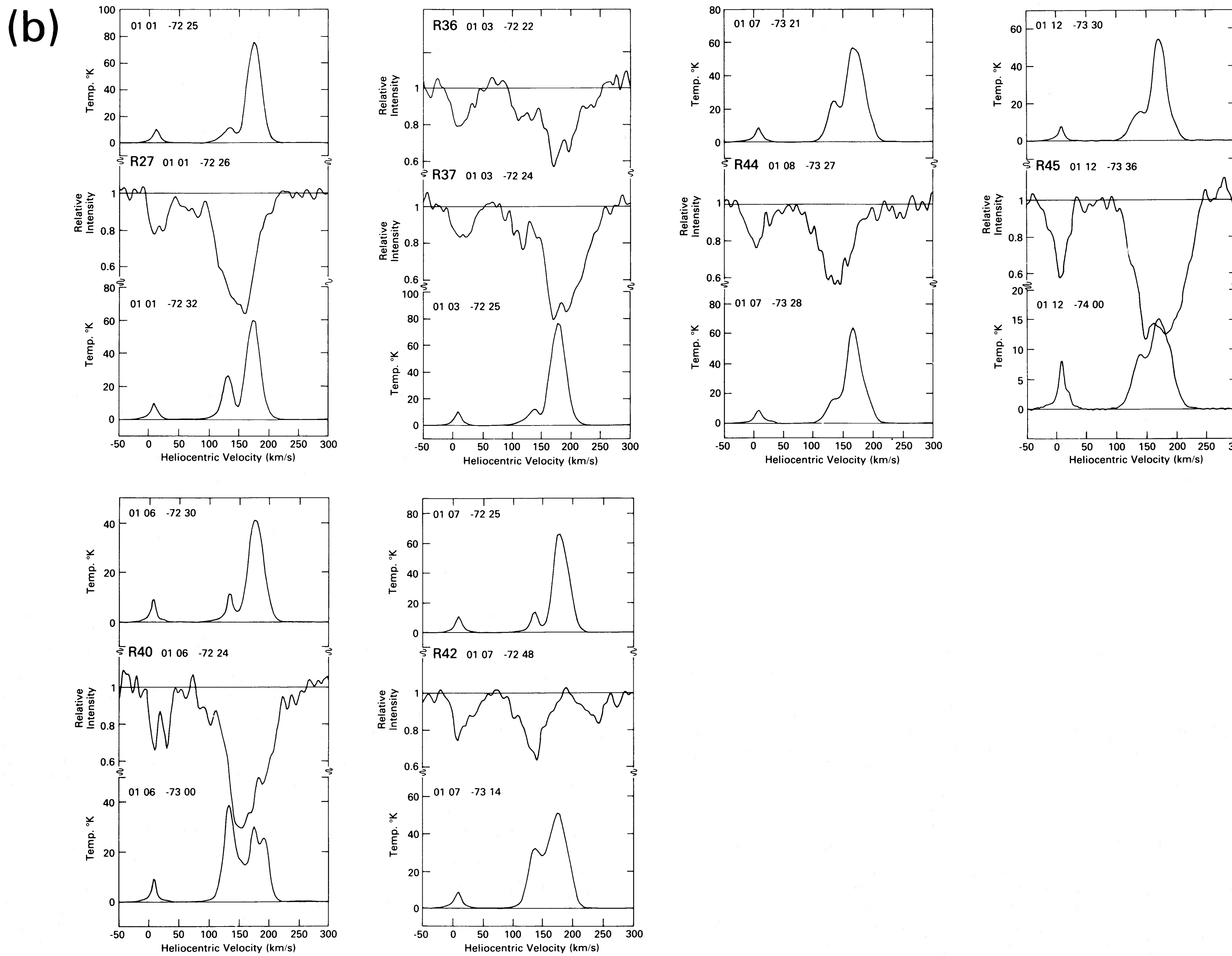

FIG. 8—*Continued*

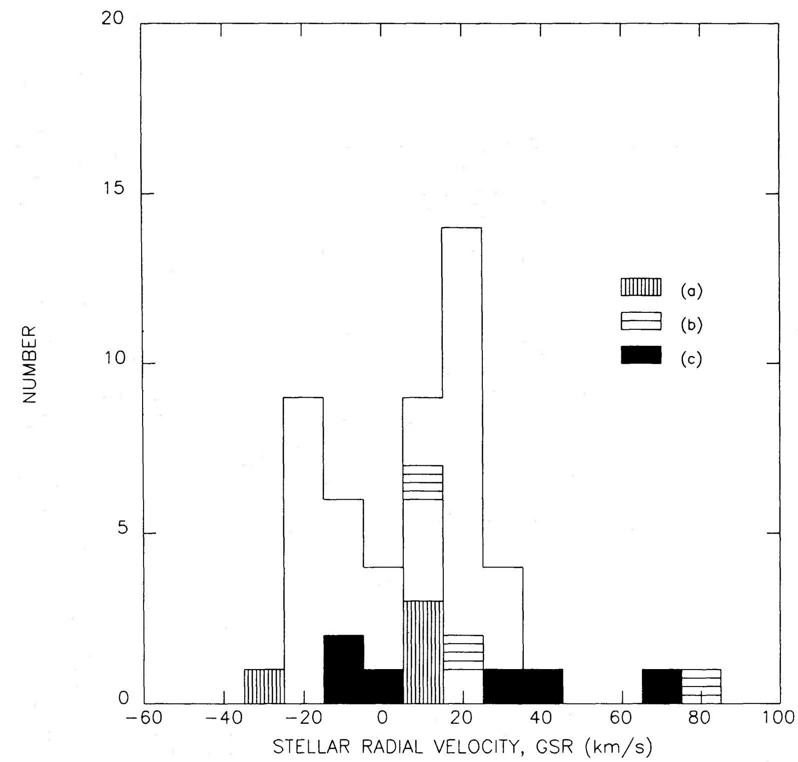

FIG. 9.—The distribution of stellar radial velocities for stars observed in the SMC. The velocities are taken from the compilation of Ardeberg and Maurice (1977), corrected for motion of the Sun with respect to the local standard of rest (20 km s^{-1}) and the Galactic center (250 km s^{-1}). The outer histogram is the distribution of early-type stars from Ardeberg and Maurice (1979) (Fig. 2 of that paper). The inner histograms show the distribution of the 18 stars of the present sample split into four groups corresponding to stars in categories (*a*), (*b*), and (*c*) (see § III) and unclassified (*blank*).

REFERENCES

Ardeberg, A., and Maruice, E. 1977, *Astr. Ap. Suppl.*, **30**, 261.
———. 1979, *Astr*, *Ap.*, **77**, 277.
Arp, H. C. 1958, *A. J.*, **63**, 118.
Azzopardi, M., and Vigneau, J. 1982, *Astr. Ap. Suppl.*, **50**, 291.
Basinski, J. M., Bok, B. J., and Bok, P. F. 1967, *M.N.R.A.S.*, **137**, 55.
Blades, J. C. 1980, *M.N.R.A.S.*, **190**, 33.
Blades, J. C., and Meaburn J. 1980, *M.N.R.A.S.*, **190**, 59p.
Blades, J. C., and Morton, D. C. 1983, *M.N.R.A.S.*, **204**, 317.
Cohen, J. G. 1981, *Ap. J.*. **247**, 869.
———. 1984, *A.J.*, **89**, 1779.
Davies, R. D., Elliott, K. H., and Meaburn, J. 1976. *Mem. R.A.S.*, **81**, 89.
de Vaucouleurs, G. 1957, *A.J.*, **62**, 69.
Feast, M. W., Thackeray, A. D., and Wesselink, A. J. 1960. *M.N.R.A.S.*, **121**, 337.
Fehrenbach, Ch., and Duflot, M. 1974, *Astr. Ap. Suppl.*, **13**, 173.
———. 1982, *Astr. Ap. Suppl.*, **48**, 409.
Feitzinger, J. V., 1980, *Space Sci. Rev.* **27**, 35.
Feitzinger, J. V., and Schmidt-Kaler, Th. 1982, *Ap. J.*, **257**, 587.
Greenstein, J. L. 1968, *Ap. J.*, **152**, 431.
Henize, K. G. 1956, *Ap. J. Suppl.*, **2**, 315.
Hindman, J. V. 1967, *Australian J. Phys.*, **20**, 147.
Howarth, I. D. 1982, *M.N.R.A.S.*, **198**, 298.
Lin, D. N. C., and Lynden-Bell, D. 1977, *M.N.R.A.S.*, **181**, 59.
———. 1982, *M.N.R.A.S.*, **198**, 707.
Mathewson, D. S., Cleary, M. N., and Murray, J. D. 1974, *Ap. J.*, **190**, 291.
Mathewson, D. S., and Ford, V. L. 1984, in *IAU Symposium 108*, *Structure and Evolution of the Magellanic Clouds*, ed. S. van den Bergh and K. S. de Boer (Dordrecht: Reidel), p. 125.
Mathewson, D. S., Ford, V. L., Schwarz, M. P., and Murray, J. D. 1979, in *IAU Symposium 84*, *The Large Scale Characteristics of the Galaxy*, ed. W. B. Burton (Dordrecht: Reidel), p. 547.
McGee, R. X., and Milton, J. A. 1966*a* *Australian J. Phys. Astr. Suppl.*, No. 2.
———. 1966*b*, *Australian J. Phys.*, **19**, 343.
McGee, R. X., and Newton, L. M. 1982*a*, *Proc. Astr. Soc. Australia*, **4**, 189.
———. 1982*b*, *Proc. Astr. Soc Australia*, **4**, 308.
McGee, R. X., Newton, L. M., and Morton, D. C. 1983, *M.N.R.A.S.*, **205**, 1191.
Murai, T., and Fujimoto, M. 1980, *Pub. Astr. Soc. Japan.* **32**, 581.
Rohlfs, K., Kreitschmann, J., Siegman, B. C., and Feitzinger, J. V. 1984, *Astr. Ap.*, **137**, 343.
Rousseau, J., Martin, N., Prévot, L., Rebeirot, E., Robin, A., and Brunet, J. P. 1978, *Astr. Ap., Suppl.*, **31**,243.
Sanduleak, N. 1968, *A.J.*, **73**, 246.
———. 1969, *A.J.*, **74**, 877.
———. 1970, *Cerro Tololo Inter-American Observatory, Contributions*, No. 89.
Savage, B. D., and de Boer, K. S. 1979, *Ap. J.* (*Letters*), **230**, L77.
———. 1981, *Ap. J.*, **243**, 460.
Songaila, A. 1981*a*, *Ap. J.* (*Letters*), **243**, L19.
———. 1981*b*, *Ap. J.*, **248**, 945.
Songailia, A., Cowie, L. L., and York, D. G. 1981, *Ap. J.*, **248**, 956.
Songaila, A., and York, D. G. 1980, *Ap. J.*, **242**, 976.
Thackeray, A. D. 1962, *M.N.A.S., So. Africa*, **21**, 74.
York, D. G. 1982, *Ann Rev. Astr. Ap.*, **20**, 221.

J. C. BLADES, L. L. COWIE, E. M. HU, and A. SONGAILA: Space Telescope Science Institute, Homewood Campus, 3700 San Martin Drive, Baltimore, MD 21218